Relativistic generalization of formation and ion reflection conditions in electrostatic shocks

A. Stockem[1],* E. Boella[1,2], F. Fiuza[1,3], and L. O. Silva[1†]

[1] *GoLP/Instituto de Plasmas e Fusão Nuclear - Laboratório Associado, Instituto Superior Técnico, Lisboa, Portugal*

[2] *Dipartimento Energia, Politecnico di Torino, Torino, Italy*

[3] *Lawrence Livermore National Laboratory, California*

(Dated: January 15, 2013)

Abstract

The theoretical model for the steady state Mach number of electrostatic shocks formed in the interaction of two plasma slabs of arbitrary density and temperature [1] is generalized for relativistic electron temperatures. We find that the relativistic correction leads to lower Mach numbers, and as a consequence, ions are reflected with lower energies. The steady state bulk velocity of the downstream population is introduced as an additional parameter to describe the transition between the minimum and maximum Mach numbers in dependence of the initial density and temperature ratios. Ion trapping and Landau damping are qualitatively discussed as dissipation mechanisms which can transform the soliton-like solution in the upstream into a shock.

PACS numbers: 47.40.Nm, 52.35.Tc, 52.38.-r

*Electronic address: anne.stockem@ist.utl.pt

†Electronic address: luis.silva@ist.utl.pt

I. INTRODUCTION

Collisionless shocks can efficiently accelerate charged particles to high energies and its study is of interest to a wide range of scenarios, e. g. space and astrophysics, especially in the context of acceleration of cosmic rays to ultra high energies (up to $\sim 10^{21}\,\mathrm{eV}$) [2], laser-plasma interactions with applications in proton therapy of tumors [3] or injection of particles for conventional accelerators [4], and inertial confinement fusion [5]. Electrostatic shocks have been observed in interplanetary space [6–8], in particular in the ionosphere [9] and in the auroral region [10], where they arise from plasma cloud collisions at the interaction between solar wind and magnetosphere or between solar wind and interstellar medium in the heliosphere region [11].

Recently, electrostatic shocks have been propelled into the focus of research due to the ability of generating high Mach numbers in compact laboratory systems [12, 13], which could provide an alternative to the costly standard synchrotron accelerators. It was found that ions are efficiently accelerated in electrostatic shocks by reflection from the electrostatic potential with twice the shock velocity in the rest frame of the upstream [14]. Shocks with moderate Mach numbers were generated in a laboratory experiment, where ion beams with 20 MeV were produced [12]. The trend towards $> 250\,\mathrm{MeV/nucleon}$ with a quasi-monoenergetic profile, which is relevant for the treatment of deep seated tumors [15], was demonstrated by particle-in-cell simulations of laser-driven shock acceleration [13].

The theoretical framework for the interaction of two plasma slabs leading to non-linear structures with large Mach numbers [16, 17] has been generalized by Sorasio et al. [1] for arbitrary plasma temperatures and densities. In this paper, we extend this work to relativistic electron temperatures and discuss efficient acceleration of ions. The conditions for shock solutions are derived from an analysis of the Sagdeev potential [18], being fully described by the ratios of the initial densities and temperatures, which also determine the condition for reflection and subsequent acceleration of ions by the electrostatic shock potential.

In section II the theoretical framework is described and the conditions for obtaining a shock-like solution are given. The dependence of the steady-state shock Mach number on the initial plasma temperature and density ratios is analyzed in section III, and the underlying characteristics leading to a minimum and a maximum value for the Mach number are investigated, considering the impact of a downstream velocity on the shock Mach number.

The conditions to obtain ion reflection and high energy ions are addressed in section IV and dissipative effects that can create the oscillatory downstream potential are discussed in section V. The results are summarized in section VI.

II. ELECTROSTATIC SHOCK SOLUTIONS FROM ARBITRARY UPSTREAM AND DOWNSTREAM DENSITIES AND TEMPERATURES

Plasmas composed of hot electrons and cold ions are governed by ion sound waves with phase velocity $\omega/k \simeq \sqrt{k_B T_e/m_i} = c_s$. The high ion inertia creates a restoring force to the thermally expanding electrons and wave steepening due to non-linear effects can lead to the generation of electrostatic shocks. Dissipative effects in the downstream region are necessary to have laminar shock solutions, in contrast to a solitary wave, and are addressed in section V. In this section, we focus on the physics in the upstream region, making use of the Sagdeev formalism [18] in order to determine the electrostatic potential.

The collision of two semi-infinite plasma slabs with arbitrary temperature and density, will lead to the formation of an electrostatic shock if the fluid velocity is small compared to the thermal velocity of the electrons. In the rest frame of the shock, the upstream population of electrons and ions is moving with v_{sh} towards the shock. An electrostatic potential is formed due to the different inertia of the particles, which is steady in time in the shock rest frame, and increases monotonically from ϕ_0 at $x = x_0$ in the far upstream until it reaches its maximum ϕ_1 at $x = x_1$, where the transition to the oscillatory downstream region is defined (see Fig. 1). The double layer is then maintained by four populations. Two populations of free electrons in the upstream and downstream regions moving towards the shock, with kinetic energies higher than the potential energy, a population of trapped electrons whose kinetic energy is less than the potential energy and a population of cold ions flowing from the upstream to the downstream region while being decelerated by the electrostatic potential.

The electron populations are treated kinetically, while the ions are treated as a fluid. The electron distributions have to be solution of the stationary Vlasov equation and can be determined knowing the particle distributions in the unperturbed plasma. The free (left) electron population, propagating from the upstream to the downstream region, is described by the relativistic drifting 1D Jüttner distribution function $f_0(\gamma_0) = N_0 \mathrm{K}_1^{-1}(\mu_0)\, \gamma_0(\gamma_0^2 -$

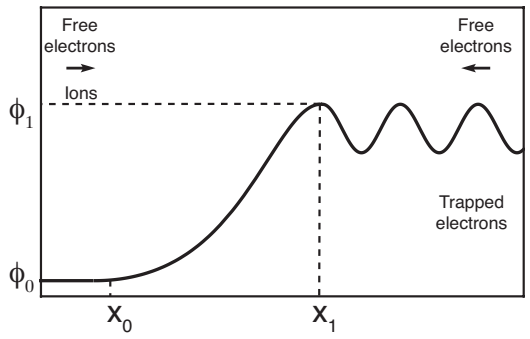

FIG. 1: Electrostatic shock formation from the interaction of free and trapped electrons and a population of cold ions. The electrostatic potential shows a monotonous increase from ϕ_0 in the upstream region ($x < x_0$) to ϕ_1 in the downstream ($x > x_1$), where it becomes oscillatory.

$1)^{-1/2} \exp[-\mu_0\gamma_0(1-\beta_0\beta_{sh})]$ [19] with the normalized velocity of the electrons $\beta_0 = v_0/c > 0$, the Lorentz factor $\gamma_0 = (1-\beta_0^2)^{-1/2}$, the thermal parameter $\mu_0 = m_e c^2/k_B T_0$, where T_0 is the electron temperature, m_e the electron mass and k_B the Boltzmann constant, and normalized fluid velocity $\beta_{sh} = v_{sh}/c$. The normalization constant contains the density of the left electron population N_0 in the upstream region ($x < x_0$) and the modified Bessel function of the second kind K_1. In the limit of nonrelativistic electron temperatures, $\mu_0 \gg 1$, the distribution function is approximated by a Maxwell-Boltzmann distribution and the thermal velocity can be introduced as $v_{th,0} = \sqrt{k_B T_0/m_e} = c/\sqrt{\mu_0}$. The free electrons in the downstream region (right population) are described by $f_1(\gamma_1) = N_1 \mathrm{K}_1^{-1}(\mu_1)\,\gamma_1(\gamma_1^2 - 1)^{-1/2} \exp\left[-\mu_1\gamma_1(1-\beta_1\beta_d) + \frac{e(\phi_1-\phi_0)}{k_B T_1}\right]$ with $\beta_1 = v_1/c < 0$, where the parameters have the same meaning as for the left population and are indicated with a subscript 1, and β_d is the fluid velocity of the downstream. To facilitate comparison with the nonrelativistic model we stick to the notation of Sorasio et al. [1] and have multiplied the distribution function by a factor containing the potential step $\phi_1 - \phi_0$. N_1 represents the density of the right electron population in the far upstream and sums up with the density of the left population to the ion density $N_i = N_0 + N_1$ at $x < x_0$ to guarantee charge neutrality. The trapped electrons are represented by the flat-top distribution function in the relativistic notation $f_{1t} = N_1 \mathrm{K}_1^{-1}(\mu_1)\,\gamma_1(\gamma_1^2 - 1)^{-1/2} \exp(-\mu_1)$, according to the so-called "maximum-density-trapping" approximation [20, 21], which guarantees $f_1(\gamma_1 = \gamma_c) = f_{1t}$ at the critical Lorentz factor $\gamma_c = 1 + e(\phi_1 - \phi_0)/m_e c^2$ that discriminates between free ($\beta_1 < -\beta_c$) and trapped

electrons ($|\beta_1| < \beta_c$), shown in Fig. 2 where the more convenient parameter $u = \beta\gamma$ has been introduced. Since the fluid velocities β_{sh} and β_d are small compared to the thermal velocities, we will neglect this dependence in the following calculations.

We introduce the electron Lorentz factor γ_e which accounts for the electrostatic potential in the shock frame and make use of the conservation of energy to write the upstream and downstream Lorentz factors as $\gamma_e = \gamma_0 + e(\phi - \phi_0)/m_e c^2 = \gamma_1 - e(\phi_1 - \phi)/m_e c^2 \geq 1$. The electron density can then be computed as $n_e = \int_1^\infty f_e(\gamma_e)\, d\gamma_e$, obtaining the electron densities in the upstream region $n_0(\Delta\varphi) = N_0\, \mathrm{K}_1^{-1}(\mu_0) \mathrm{e}^{\Delta\varphi} \int_{1+\Delta\varphi/\mu_0}^\infty \mathrm{e}^{-\mu_0\gamma_e} \gamma_e(\gamma_e^2-1)^{-1/2}\, d\gamma_e$ and downstream region $n_1(\Delta\varphi) = N_0 \Gamma \mathrm{K}_1^{-1}(\mu_0/\Theta) \left[\mathrm{e}^{\Delta\varphi/\Theta} \int_{1+\Delta\varphi/\mu_0}^\infty \mathrm{e}^{-\mu_0\gamma_e/\Theta} \gamma_e(\gamma_e^2-1)^{-1/2}\, d\gamma_e + 2\mathrm{e}^{-\mu_0/\Theta} \sqrt{(1+\Delta\varphi/\mu_0)^2 - 1}\right]$ with the dimensionless quantities $\Delta\varphi = e(\phi - \phi_0)\mu_0/m_e c^2$, $\Gamma = N_1/N_0$ and $\Theta = \mu_0/\mu_1$.

Using the fluid equations for ion mass and energy conservation and assuming that the ions are cold and that none of them is reflected at the potential, the ion density can be determined as $n_i(\Delta\varphi) = N_i/\sqrt{1 - 2\,\Delta\varphi/M^2}$, where $M = v_{sh}/c_s$ is the ion acoustic Mach number, $c_s = \sqrt{k_B T_0/m_i}$ the upstream ion sound speed and m_i is the ion mass. The particle densities are then combined in Poisson's equation

$$\frac{\mathrm{d}^2\Delta\varphi}{\mathrm{d}\chi^2} = -\frac{n_i(\Delta\varphi)}{N_i} + \frac{n_0(\Delta\varphi) + n_1(\Delta\varphi)}{N_i}, \tag{1}$$

where the normalized quantity $\chi = x/\lambda_D$ with $\lambda_D = \sqrt{K_B T_0/(4\pi e^2 N_i)}$ has been introduced. Defining the right hand side of equation (1) as $-\mathrm{d}\Psi(\Delta\varphi)/\mathrm{d}\Delta\varphi$, the similarity to the har-

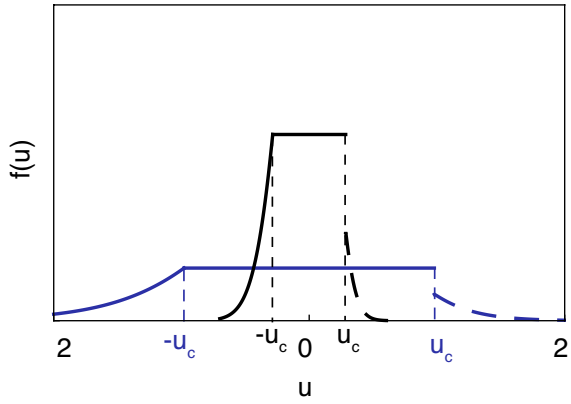

FIG. 2: Electron distribution functions upstream (f_0 – dashed) and downstream ($f_1 + f_{1t}$ – solid) for two different electron temperatures $\mu_0 = 5$ (blue) and 50 (black) with $\Gamma = 3$, $\Theta = 2$, $e(\phi_1 - \phi_0)/m_e c^2 = 2$ and $\beta_{sh} = 0.02$.

monic oscillator can be immediately noticed and equation (1) can be seen as the motion of a pseudo-particle in the Sagdeev potential $\Psi(\Delta\varphi)$ [18], allowing to identify bounded solutions as possible shock solutions. Integration of equation (1) with respect to $\Delta\varphi$ leads to

$$\frac{1}{2}\left(\frac{\mathrm{d}\Delta\varphi}{\mathrm{d}\chi}\right)^2 + \Psi(\Delta\varphi) = const =: \Psi_0 \tag{2}$$

with $\Psi_0 = \Psi(\varphi_0, M, \Gamma, \Theta)$ and the non-linear Sagdeev potential given by

$$\Psi(\Delta\varphi, M, \Gamma, \Theta) = P_i(\Delta\varphi, M) - P_{e0}(\Delta\varphi, \Gamma) - P_{e1}(\Delta\varphi, \Gamma, \Theta) \tag{3}$$

where the quantities P_i, P_{e0} and P_{e1} represent the ion, the upstream electron and the downstream electron pressures, respectively, which are defined as

$$P_i(\Delta\varphi, M) = M^2\left(1 - \sqrt{1 - \frac{2\Delta\varphi}{M^2}}\right) \tag{4}$$

$$P_{e0}(\Delta\varphi, \Gamma, \mu_0) = \frac{1}{1+\Gamma}\left[\frac{\mu_0}{K_1(\mu_0)}\int_1^\infty d\gamma\, \mathrm{e}^{-\mu_0\gamma}\sqrt{\left(\gamma + \frac{\Delta\varphi}{\mu_0}\right)^2 - 1} - 1\right] \tag{5}$$

$$\begin{aligned} P_{e1}(\Delta\varphi, \Gamma, \Theta, \mu_0) = \frac{\Gamma\Theta}{1+\Gamma}\Bigg[&\frac{\mu_0 \mathrm{e}^{-\mu_0/\Theta}}{\Theta K_1(\mu_0/\Theta)}\left\{\int_1^\infty d\gamma\, \mathrm{e}^{-\mu_0(\gamma-1)/\Theta}\sqrt{\left(\gamma + \frac{\Delta\varphi}{\mu_0}\right)^2 - 1}\right. \\ &\left. + s\sqrt{s^2-1} - \log\left[s + \sqrt{s^2-1}\right]\right\} - 1\Bigg] \end{aligned} \tag{6}$$

with $s = 1 + \Delta\varphi/\mu_0$. In the case of nonrelativistic temperatures, $\mu_0 \gg 1$, equations (5) and (6) can be integrated analytically, retrieving the expressions of [1]

$$P_{e0}^{nr}(\Delta\varphi, \Gamma) = \frac{1}{1+\Gamma}\left(\frac{2\sqrt{\Delta\varphi}}{\sqrt{\pi}} + \mathrm{e}^{\Delta\varphi}\,\mathrm{erfc}\,\sqrt{\Delta\varphi} - 1\right) \tag{7}$$

$$P_{e1}^{nr}(\Delta\varphi, \Gamma, \Theta) = \frac{\Theta\Gamma}{1+\Gamma}\left(\frac{2}{\sqrt{\pi}}\sqrt{\frac{\Delta\varphi}{\Theta}} + \mathrm{e}^{\frac{\Delta\varphi}{\Theta}}\,\mathrm{erfc}\,\sqrt{\frac{\Delta\varphi}{\Theta}} + \frac{8}{3\sqrt{\pi}}\Delta\varphi\sqrt{\frac{\Delta\varphi}{\Theta^3}} - 1\right) \tag{8}$$

with erfc the complimentary error function. Note that the explicit dependence on the upstream and downstream temperatures vanishes in this approximation. For highly relativistic electron temperatures, $\mu_0 \ll 1$, the pressures are approximated by

$$P_{e0}^{r}(\Delta\varphi, \Gamma) = \frac{\Delta\varphi(1-\mu_0)}{1+\Gamma} \tag{9}$$

$$P_{e1}^{r}(\Delta\varphi, \Gamma, \Theta) = \frac{\Delta\varphi\Gamma}{\Theta(1+\Gamma)}\left[\Delta\varphi\left(1 - \frac{\mu_0}{\Theta}\right) + \Theta\left(1 + \frac{\mu_0}{\Theta}\right)\right] \tag{10}$$

and the explicit dependence on the temperatures is still maintained. Figure 3 shows the

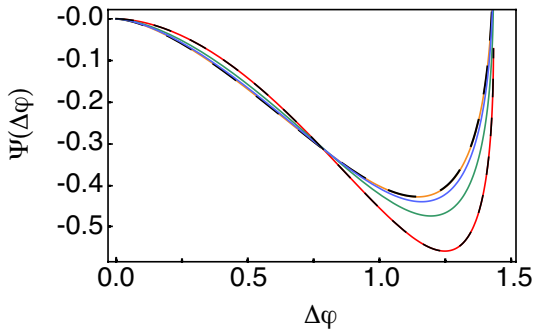

FIG. 3: Sagdeev potential $\Psi(\varphi)$ obtained from equations (3)-(6) for $M = 1.7$, $\Gamma = 3$, $\Theta = 1$ and $\mu_0 = 0.1$ (red), 1 (green), 5 (blue), 100 (orange). Represented by dashed lines are the non-relativistic and highly relativistic approximations, given by equations (7)-(10).

Sagdeev potential, given by equations (3)-(6), for upstream electron temperatures $\mu_0 = 0.1 - 100$ for a constant Mach number M and a comparison with the nonrelativistic and highly relativistic approximations (7)-(10). A higher temperature leads to larger absolute values of the minimum of Ψ, which results in lower values for the Mach number at which ion reflection sets in, as will be shown in the following section.

III. MACH NUMBER DEPENDENCE ON INITIAL PARAMETERS

As can be seen from equation (4), the model holds for $\Delta\varphi < M^2/2 := \Delta\varphi_{cr}$. The ion pressure becomes imaginary when the electrostatic potential exceeds the ion kinetic energy

$$e\Delta\phi > \frac{1}{2} m_i v_i^2 \tag{11}$$

and the ions are reflected by the shock potential. We define the Mach number at which ion reflection sets in as the maximum Mach number M_{max}. In order to determine possible shock solutions with M_{max}, we use equation (2) which gives the condition for the existence of a monotonic double layer solution as $\tilde{\Psi} := \Psi(\Delta\varphi, M, \Gamma, \Theta) - \Psi_0 < 0$. For a given Mach number M, a soliton-like solution is possible only if the electron pressure exceeds the ion pressure. The solutions are found numerically by solving $\tilde{\Psi}(M^2/2, M, \Gamma, \Theta) = 0$ and are shown in figure 4.

As already found in [1], the analytical dependence of the maximum Mach number in the

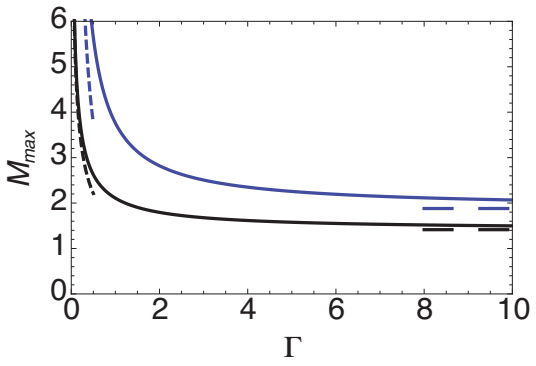

FIG. 4: Maximum Mach number versus density ratio for the highly relativistic case $\mu_0 = 0.1$ (black) given by Eq. (12) and the non-relativistic case given in [1] (blue) for a temperature ratio $\Theta = 1$. The dependences for very small and very large density ratios are indicated by the dashed lines.

non-relativistic approximation is given by $M_{max} = 3\sqrt{\pi\Theta/8}(1+\Gamma)/\Gamma$, which is $M_{max} \approx 3\sqrt{\pi\Theta/8}$ for large density ratios and has a $M_{max} \propto \Gamma^{-1}$ dependence for low density ratios. Here, we find for the case of highly relativistic temperatures, $\mu_0 \ll 1$,

$$M_{max} = \sqrt{2\Theta\left(1 + \frac{1+\mu_0}{\Gamma(1-\mu_0/\Theta)}\right)}, \tag{12}$$

which is displayed in figure 4 together with the non-relativistic expression. It can be easily seen that the maximum Mach number is constant for high density ratios as in the non-relativistic case, $M_{max} \approx \sqrt{2\Theta}$ for $\Gamma \gg 1$, and has a dependence $M_{max} \approx \sqrt{2\Theta(1+\mu_0)/\Gamma(1-\mu_0/\Theta)} \propto \Gamma^{-1/2}$ for $\Gamma \ll 1$. The comparison of the non-relativistic and highly relativistic cases in figure 4 for a temperature ratio $\Theta = 1$ shows that for higher upstream electron temperatures the maximum Mach number is reduced.

We analyze now the lower limit and the range of possible Mach numbers for given temperature and density ratios. The shape of the Sagdeev potential and thus the existence of shock solutions depends on the choice of Γ and Θ and we can distinguish three different types of solutions which are shown in Figure 5. Case (1) represents the case where shock solutions exist for $\tilde{\Psi} = \Psi - \Psi_0 < 0$ and $\Delta\varphi > 0$. While the monotonously growing Sagdeev potential in case (3) does not allow for shock solutions, case (2) defines the threshold with $\Delta\varphi = 0$ and provides the conditions to determine the minimum Mach number, which are given by $d\tilde{\Psi}/d\Delta\varphi = 0$ and $\tilde{\Psi}(\Delta\varphi) = 0$. While in the highly relativistic limit $M = 1$ is the lower limit, in the non-relativistic case a lower limit $M > 1$ exists. The Sagdeev potential

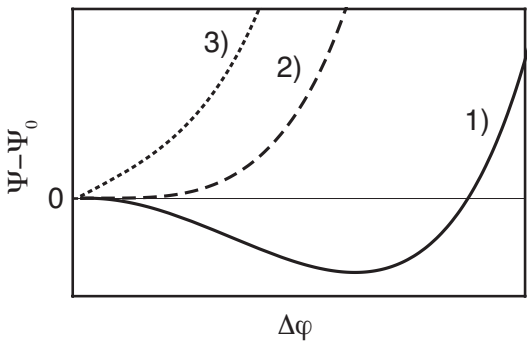

FIG. 5: Different types of the Sagdeev potential $\tilde{\Psi}(\Delta\varphi) = \Psi - \Psi_0$.

is expanded for $\Delta\varphi \ll 1$ since we are looking for solutions $\Delta\varphi \to 0$, obtaining

$$\tilde{\Psi}(\Delta\varphi, M, \Gamma, \Theta) \approx \Delta\varphi^2 \left[\frac{1}{2M^2(1-\frac{2\varphi_0}{M^2})^{3/2}} + \frac{1}{2(1+\Gamma)} \left(\frac{1-\Gamma\Theta^{-1/2}}{\sqrt{\varphi_0 \pi}} - e^{\varphi_0}\mathrm{erfc}(\sqrt{\varphi_0}) - \frac{\Gamma}{\Theta} e^{\varphi_0/\Theta}\mathrm{erfc}(\sqrt{\frac{\varphi_0}{\Theta}}) \right) \right], \quad (13)$$

which is a function of the upstream potential φ_0. The minimum Mach number can then be found by solving $\tilde{\Psi}(\Delta\varphi, M(\varphi_0), \Gamma, \Theta) = 0$ with the Mach number at the minimum of the Sagdeev potential given by

$$M(\varphi_0) = \sqrt{2\varphi_0} \Big/ \left\{ 1 - \frac{(1+\Gamma)^2}{\left[e^{\varphi_0}\mathrm{erfc}[\sqrt{\varphi_0}] + \Gamma \left(4\sqrt{\frac{\varphi_0}{\pi\Theta}} + e^{\varphi_0/\Theta}\mathrm{erfc}[\sqrt{\varphi_0/\Theta}] \right) \right]^2} \right\}^{1/2}. \quad (14)$$

For large temperature ratios we find small deviations from the approximation $\varphi_0 = 0$ [1], which is equivalent to $\Psi_0 = 0$ in equation (2), see Figure 6 (a). Panel (b) shows the respective Sagdeev potentials with $\Psi_0 = 0$ for the minimum Mach number according to $\Delta\varphi = 0$ in black and for the approximated model with $\varphi_0 = 0$ in red. The exact solution allows for the formation of electrostatic shocks at slightly lower Mach numbers.

The transition between minimum and maximum Mach number can be described as a function of the steady state ion speed in the downstream region, v_d. In the rest frame of the shock, the upstream ions propagate towards the shock with velocity $v_{i,us} := v_{sh}$ and are decelerated by the shock potential φ to velocities in the downstream $0 \leq v_{i,ds} \leq v_{sh}$. The velocity is $v_{i,ds} = 0$ if the ions are completely stopped by the potential and $v_{i,ds} = v_{sh}$ if they are unaffected and stream freely in the downstream region. In the upstream frame this corresponds to ion downstream velocities $-v_i \leq v_{i,du} := -v_d \leq 0$. Starting once more from

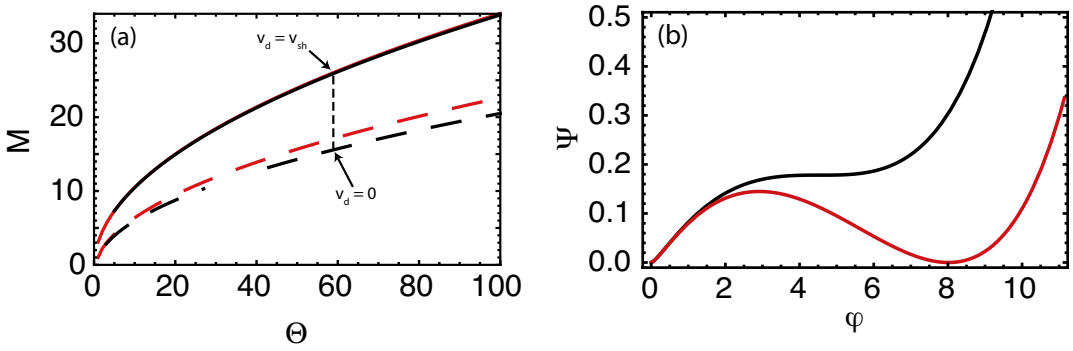

FIG. 6: (a) M_{min} (dashed) and M_{max} (solid) for the approximation $\varphi_0 = 0$ (red) and comparison with the exact solution (black) for $\Gamma = 1$. The dashed vertical line shows the transition from M_{min} to M_{max} for downstream velocities $0 \leq v_d \leq v_{sh}$. (b) Sagdeev potential for the minimum Mach number with $\Delta\varphi = 0$ (black) and comparison with the approximation $\varphi_0 = 0$ (red).

the energy conservation for ions, we can relate the downstream ion speed directly with the shock potential $v_d/c_s = M - \sqrt{M^2 - 2\Delta\varphi}$ and use

$$\Delta\varphi_d := \frac{M^2}{2}\left[1 - \left(1 - \frac{v_d}{v_{sh}}\right)^2\right] \tag{15}$$

to find the zeros of the Sagdeev potential $\tilde{\Psi}(\Delta\varphi_d, M, \Gamma, \Theta)$ to determine the Mach number M. This transition is shown in figure 6a. When the shock propagates with a speed slightly above the minimum Mach number, the downstream will have almost the same speed as the upstream population due to the small potential jump that has only a weak effect on the particles. At the maximum Mach number, the potential jump is so strong that the downstream propagates with the same speed as the shock front.

IV. ION REFLECTION FROM THE ELECTROSTATIC POTENTIAL

In the context of applications of shock-accelerated ions, e. g. for medical purposes, it is important to achieve high energies and the realization of the theory is restricted by experimental feasibility. As shown in Fiuza et al. (2012) [13], for typical experimental conditions associated with laser-driven shocks, ion acceleration occurs close to the critical Mach number $M \approx M_{cr}$, so that the reflected ions will have a velocity $v_{i,refl} = 2v_{sh} = 2M_{cr}c_s$, which is determined by the condition for the critical Mach number. To simply reflect ions

from the shock, figures 4 and 6a show that large density ratios Γ and low temperature ratios Θ are favorable, since low Mach number shocks are easier to drive.

In order to achieve high energy ions, large Mach numbers M_{cr} and/or large ion sound speeds c_s are needed. An increase in the Mach number can be gained by a high initial temperature ratio Θ, which is equivalent with increasing the energy of the slabs for a fixed upstream c_s, and a high piston velocity, which provides a high momentum transfer to the plasma (i. e. initial relative fluid velocity between the two slabs) [22]. The sound speed can be increased by increasing the actual value of the electron temperature. This works well in near-critical density plasmas as a significant fraction of the laser energy can be absorbed by the plasma [13].

V. DISSIPATIVE EFFECTS LEADING TO AN OSCILLATORY DOWNSTREAM POTENTIAL

So far, we have described the solitary solution in the upstream region and neglected the processes leading to a shock solution. The inclusion of a constant population of trapped electrons in the downstream region is not enough to break the symmetry. In this section, we qualitatively discuss possible mechanisms that lead to shock formation, which are ion trapping in the downstream of the shock and electron Landau damping.

It is assumed that ions are reflected from the shock front, which leads to an electrostatically stable solution only if the fraction of reflected ions is small and wave-particle interactions are negligible. Moreover, ion trapping in the downstream region can also be important. The electrostatic potential in the upstream region is then given by the soliton solution derived in the previous section. The downstream potential is described by a second Sagdeev potential, which considers the physics in this region, by applying for example the Bernstein-Greene-Kruskal (BGK) method [23], where the oscillatory electrostatic potential is separated into individual sections with each section considering the trapping of a different species. Figure 7 shows a sketch of the ion phase space (v, x) to illustrate this approach. Ions entering the shock region from the upstream are decelerated to $v < v_i$, and can enter the downstream region only if the initial kinetic energy exceeds the electrostatic energy. Trapped ions in the downstream have a kinetic energy smaller than the potential energy and their phase spaces are closed. To derive the Sagdeev potential, the downstream is split into

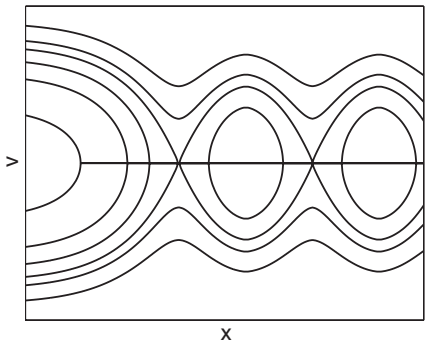

FIG. 7: Ion phase space showing free and trapped populations

several sections and the energy distribution of trapped and untrapped ions and electrons is considered in each region.

If the fraction of reflected ions is small, the upstream potential is not affected by the actual shape of the downstream potential [24]. Using the analogy of the harmonic oscillator, the electrostatic potential swings in the first Sagdeev potential until it reaches the maximum ϕ_{max}, entering then the second Sagdeev potential, where it does the continuous oscillatory motion. The conditions to match the potentials require therefore $\Psi_I = \Psi_{II}$ and φ and $\partial\varphi/\partial x$ to be continuous at $\varphi = \varphi_{max}$.

Our analysis throughout this paper focusses on the regime, where ion reflection is not present yet and provides the condition for ion reflection. An alternative way how to introduce dissipation and to break the soliton symmetry in this Mach number range, is taking into account Landau damping of electrons. The solitary electrostatic potential accelerates the electrons while propagating towards the peak and a considerable amount of electrons will have velocities around the resonance condition $v_e \simeq v_{ph} = c_s$. The interaction with ion acoustic waves leads to acceleration of particles with velocities $v_e \lesssim c_s$ and deceleration of particles with velocities $v_e \gtrsim c_s$. As the number of particles with velocities $v_e \lesssim c_s$ is higher than the number of particles with velocities $v_e \gtrsim c_s$, the waves will be damped. Landau damping of ions can become important if the ions are also trapped in the downstream potential. The consequence of this wave damping is a polynomial solution for the Sagdeev potential [25], which gives a shock-like solution for the electrostatic potential [24].

VI. SUMMARY

In this paper, electrostatic shock solutions have been identified starting from an initial system of two colliding plasma slabs, containing two populations of hot electrons and cold ions and a population of trapped electrons. From the calculation of the pressure terms, the Sagdeev potential has been derived from the initial conditions for arbitrary density and temperature ratios, and a range for the steady state Mach number was presented for the stage where ion reflection starts to become important. For the first time, relativistic electron temperatures have been considered and approximations for the highly relativistic case have been presented. By introducing the steady state bulk velocity of the downstream population, an actual dependence of the Mach number on the initial density and temperature ratios was gained, bridging the range between the minimum and maximum Mach numbers. The critical Mach number at which ion reflection appears, is achieved by increasing the electron temperature in the upstream plasma, which will lead to an increase of the sound speed c_s and produce shock reflected ions with high energy.

The solitary wave in the upstream is transformed into a shock solution if dissipative effects are taken into account that will break the symmetry. Such effects are for example the trapping of electrons and ions in the downstream, which can be theoretically described with the BGK approach, or the reflection of ions from the shock front, both described by a separate Sagdeev potential for the downstream. Also Landau damping can provide the necessary dissipation. The result is an oscillatory component in the downstream electrostatic potential.

Acknowledgments

This work was partially supported by the European Research Council (ERC-2010-AdG Grant 267841) and FCT (Portugal) grants SFRH/BPD/65008/2009, SFRH/BD/38952/2007, and PTDC/FIS/111720/2009. We would like to thank Prof. Gianni

Coppa from Politecnico di Torino for fruitful discussions.

[1] G. Sorasio, M. Marti, R. A. Fonseca, and L. O. Silva, Physical Review Letters **96**, 045005 (2006).

[2] D. Caprioli, P. Blasi, and E. Amato, Astroparticle Physics **34**, 447 (2011).

[3] S. V. Bulanov, T. Z. Esirkepov, V. S. Khoroshkov, A. V. Kuznetsov, and F. Pegoraro, Physics Letters A **299**, 240 (2002).

[4] K. Krushelnick, E. L. Clark, R. Allott, F. N. Beg, C. N. Danson, A. Machacek, V. Malka, Z. Najmudin, D. Neely, P. A. Norreys, et al., IEEE Transactions on Plasma Science **28**, 1110 (2000).

[5] M. Roth, T. E. Cowan, M. H. Key, S. P. Hatchett, C. Brown, W. Fountain, J. Johnson, D. M. Pennington, R. A. Snavely, S. C. Wilks, et al., Physical Review Letters **86**, 436 (2001).

[6] P. A. Lindqvist, G. T. Marklund, and L. G. Blomberg, Space Science Review **70**, 593 (1994).

[7] B. Holback, S.-E. Jansson, L. Åhlén, G. Lundgren, L. Lyngdal, S. Powell, and A. Meyer, Space Science Review **70**, 577 (1994).

[8] M. Temerin, M. Woldorff, and F. S. Mozer, Physical Review Letters **43**, 1941 (1979).

[9] E. G. Shelley, R. D. Sharp, and R. G. Johnson, Geophys. Res. Lett. **3**, 654 (1976).

[10] C. W. Carlson, J. P. McFadden, R. E. Ergun, M. Temerin, W. Peria, F. S. Mozer, D. M. Klumpar, E. G. Shelley, W. K. Peterson, E. Moebius, et al., Geophys. Res. Lett. **25**, 2017 (1998).

[11] S. M. Krimigis, R. B. Decker, M. E. Hill, T. P. Armstrong, G. Gloeckler, D. C. Hamilton, L. J. Lanzerotti, and E. C. Roelof, Nature **426**, 45 (2003).

[12] D. Haberberger, S. Tochitsky, F. Fiuza, C. Gong, R. A. Fonseca, L. O. Silva, W. B. Mori, and C. Joshi, Nature Physics **8**, 95 (2012).

[13] F. Fiúza, A. Stockem, E. Boella, R. Fonseca, L. O. Silva, D. Haberberger, S. Tochitsky, C. Gong, W. Mori, and C. Joshi, Phys. Rev. Lett **109**, 215001 (2012).

[14] L. O. Silva, M. Marti, J. R. Davies, R. A. Fonseca, C. Ren, F. S. Tsung, and W. B. Mori, Physical Review Letters **92**, 015002 (2004).

[15] U. Linz and J. Alonso, Physical Review Special Topics Accelerators and Beams **10**, 094801 (2007).

[16] D. W. Forslund and C. R. Shonk, Phys. Rev. Lett. **25**, 1699 (1970).

[17] D. W. Forslund and J. P. Freidberg, Phys. Rev. Lett. **27**, 1189 (1971).

[18] R. Z. Sagdeev, *Review of Plasma Physics*, vol. 4 (Consultans Bureau, 1966).

[19] M. Lazar, A. Stockem, and R. Schlickeiser, Open Plasma Phys. J. **3**, 138 (2010).

[20] H. Schamel, Journal of Plasma Physics **14**, 905 (1972).

[21] D. Montgomery and G. Joyce, Journal of Plasma Physics **3**, 1 (1969).

[22] F. Fiuza, A. Stockem, E. Boella, R. A. Fonseca, L. O. Silva, D. Haberberger, S. Tochitsky, W. B. Mori, and C. Joshi, submitted to Phys. Plasmas (2012).

[23] I. B. Bernstein, J. M. Greene, and M. D. Kruskal, Physical Review **108**, 546 (1957).

[24] D. Tidman and N. Krall, *Shock waves in collisionless plasmas* (Wiley-Interscience, New York, 1971).

[25] E. Ott and R. Sudan, Phys. Fluids **13**, 1432 (1970).